

Article

Calculation of BaGa₄Se₇ OPO/OPA Output Spectrum Characteristics

Yu Liu ^{1,2}, Tianjian Wan ^{1,2}, Zhiyong Li ¹, Ziren Zhu ^{1,2}, Jinzhou Bai ^{1,2}, Juntao Tian ^{1,2}, Hai Wang ^{1,2}, Yue Lu ¹, Xinjun Su ³, Rongqing Tan ^{1,2}, Changjun Ke ¹ and Yijun Zheng ^{1,2,*}

- ¹ Aerospace Information Research Institute, Chinese Academy of Sciences, Beijing 100094, China; liuyu211@mails.ucas.ac.cn (Y.L.); wantianjian23@mails.ucas.ac.cn (T.W.); zhiyongli@mail.ie.ac.cn (Z.L.); zr_zhu@mail.ie.ac.cn (Z.Z.); baijinzhou19@mails.ucas.ac.cn (J.B.); tianjuntao18@mails.ucas.edu.cn (J.T.); wanghai21@mails.ucas.ac.cn (H.W.); luyue@aircas.ac.cn (Y.L.); rqtan@mail.ie.ac.cn (R.T.); cjke@mail.ie.ac.cn (C.K.)
- ² School of Electronic, Electrical and Communication Engineering, University of Chinese Academy of Sciences, Beijing 101408, China
- ³ Science and Technology on Particle Transport and Separation Laboratory, Tianjin 300180, China; suxinjun@ipce.cn
- * Correspondence: yjzheng@mail.ie.ac.cn

Abstract: Optical parametric oscillation (OPO) or optical parametric amplification (OPA) systems offer significant potential for generating high-energy, narrow-pulse laser output, finding applications across various domains. To achieve efficient amplification in cascade with amplifiers, precise frequency domain matching between OPO/OPA systems and amplifiers is imperative. Therefore, preliminary simulation and computation of the spectral characteristics of OPO/OPA systems are of paramount importance in the early stages of experimentation. Currently, the calculation of OPO/OPA output spectrum characteristics is limited to estimating the influence of pump light characteristics on output spectrum linewidth, a consideration that remains incomplete. This paper presents a comprehensive computational approach that takes into account the impact of four crucial factors on the output spectrum characteristics: pump light linewidth, pump light divergence angle, the walk-off effect, and the absorption loss of the crystal. This method finely characterizes the features of the output spectrum. The results obtained through the proposed approach align well with experimental results, underscoring its effectiveness. This study aims to obtain the output spectrum characteristics of BaGa₄Se₇ OPO/OPA through calculations to provide theoretical guidance for subsequent cascade amplification experiments.



Citation: Liu, Y.; Wan, T.; Li, Z.; Zhu, Z.; Bai, J.; Tian, J.; Wang, H.; Lu, Y.; Su, X.; Tan, R.; et al. Calculation of BaGa₄Se₇ OPO/OPA Output Spectrum Characteristics. *Photonics* **2023**, *10*, 1168. <https://doi.org/10.3390/photonics10101168>

Received: 19 September 2023
Revised: 14 October 2023
Accepted: 17 October 2023
Published: 20 October 2023



Copyright: © 2023 by the authors. Licensee MDPI, Basel, Switzerland. This article is an open access article distributed under the terms and conditions of the Creative Commons Attribution (CC BY) license (<https://creativecommons.org/licenses/by/4.0/>).

Keywords: BaGa₄Se₇ crystal; optical parametric amplifier (OPA); spectrum characteristics

1. Introduction

The 3–20 μm mid-infrared and far-infrared laser has important applications in biomedicine, atmospheric monitoring, remote sensing, and infrared countermeasures [1–5]. Nonlinear frequency conversion techniques play a vital role in generating 3–20 μm wavelengths. By employing nonlinear crystals in optical parametric oscillation (OPO) or optical parametric amplification (OPA) technology, parametric down-conversion can be achieved, thus extending the near-infrared wave to the mid-infrared and far-infrared spectrum. At present, the nonlinear crystals capable of generating mid to far-infrared lasers using OPO/OPA technology include AgGaS₂, AgGaSe₂, ZnGeP₂, and BaGa₄Se₇. However, AgGaS₂ and AgGaSe₂ have low damage thresholds, restricting the generation of high-energy lasers. While ZnGeP₂ possesses a large nonlinear coefficient, it also exhibits absorption below 2 μm and above 12 μm. As a result, it can only be pumped by lasers above 2 μm and cannot generate far-infrared lasers due to transmittance limitations [6]. The recently reported infrared crystal BaGa₄Se₇ exhibits promising characteristics, including a high damage threshold (557 MW/cm²), a wide transmission range (0.47–18 μm), and a large nonlinear coefficient ($d_{11} = 24.3$ pm/V) [7–10]. These attributes render BaGa₄Se₇ a potential

candidate for generating 18 μm far-infrared lasers. However, challenges arise due to the influence of the growth size, damage threshold, and quantum conversion efficiency of long-wave infrared crystals, making it difficult to achieve large-energy short-pulse output from long-wave OPO/OPA. To overcome this limitation, cascading OPO/OPA systems with amplifiers is an essential approach to achieve high-energy, narrow-pulse laser output. Research has demonstrated that BaGa_4Se_7 -OPO/OPA exhibits a broad spectrum in the long-wave range [11,12], qualifying it as a suitable seed for various gain medium amplifiers to achieve a high-energy, short-pulse, long-wave laser. And due to the wide spectrum, BaGa_4Se_7 -OPO/OPA is expected to have potential applications in ultrafast lasers [13–18].

In order to achieve effective amplification of the BaGa_4Se_7 -OPO/OPA seed source, the seed source and amplifier need to be accurately matched in the frequency domain during the cascade-amplification process. However, the research on the spectral characteristics of BaGa_4Se_7 -OPO/OPA is currently insufficient. In 1990, Bosenberg conducted a study exploring the influence of the pump light linewidth and divergence angle on the output spectrum [19]. However, this study was limited to an estimation of the broadening of the output spectral linewidth, which was assumed to be uniform, and did not provide detailed characteristics of the output spectrum. Subsequent research efforts have often referenced Bosenberg's estimation formula but have not undertaken further exploration into the simulation calculations of the output spectrum in OPO/OPA systems. In 2022, Tian et al. achieved a tunable femtosecond optical parametric amplification utilizing a BaGa_4Se_7 crystal [12]. They employed a 250 fs 1030 nm Yb: KGW laser as the pump source and focused a small portion of it into a YAG crystal, generating a stable supercontinuum through single filamentation. This supercontinuum served as the signal light, while angle tuning enabled the generation of idler light in the range of 3.7–17 μm . However, Tian et al. did not provide an extensive account of the calculation process for the simulated spectrum given in the article. To fill the gap in the field, this paper conducts a theoretical exploration of the output spectral characteristics of BaGa_4Se_7 -OPO/OPA.

The research presented in this article reveals that the output spectrum characteristics are influenced not only by the linewidth and divergence angle of the pump light but also by the walk-off effect and the inherent properties of the crystal. Furthermore, through numerical calculations, it has been established that the impact of the pump light on the output spectrum results in non-uniform spectral broadening. Consequently, relying solely on the two characteristics of the pump light for estimating uniform spectral broadening of the output spectrum is insufficient for obtaining a more accurate representation of the output spectrum, which encompasses detailed characteristics and closely aligns with the experimental results. Addressing the aforementioned shortcomings, this paper introduces a comprehensive calculation method that takes into account the linewidth of the pump light, the divergence angle of the pump light, the walk-off effect, and the absorption loss of the crystal. This method refines the phase-matching relationship using the micro-element method and enhances the previous estimation approach. It provides a more accurate assessment of how pump light characteristics impact the distribution of the output spectrum. In addition to considering the linewidth and divergence angle of the pump light [19], this method also incorporates the influence of the walk-off effect and crystal absorption loss on the output spectrum. Through numerical calculations, the cumulative effects of these four distinct factors on the output spectrum characteristics are superimposed and computed, resulting in calculated outcomes that closely align with experimental results. Comparative analysis demonstrates that the method proposed in this paper can accurately compute output spectra that closely match experimental data. This method effectively meets the demands of frequency-domain matching research in cascade amplification experiments involving long-wave OPO/OPA systems, providing precise spectrum selection for matching purposes.

2. Theoretical Basis

2.1. Phase-Matching Angle

The energy-conservation condition is followed in the optical parameter process:

$$\frac{1}{\lambda_p} = \frac{1}{\lambda_s} + \frac{1}{\lambda_i} \tag{1}$$

BaGa₄Se₇ is a biaxial crystal, which satisfies the refractive index equation of a biaxial crystal in refractive index coordinates [20]:

$$\frac{\sin^2 \theta \cos^2 \varphi}{n^{-2} - n_x^{-2}} + \frac{\sin^2 \theta \sin^2 \varphi}{n^{-2} - n_y^{-2}} + \frac{\cos^2 \theta}{n^{-2} - n_z^{-2}} = 0 \tag{2}$$

This paper simulates and calculates the output spectrum of BaGa₄Se₇-OPA to facilitate comparison with the measured spectrum in the study by Tian et al. [12]. The simulation parameters are consistent with the experimental parameters reported by Tian et al.: using the Type-I phase-matching, the pump source wavelength is chosen to be 1030 nm, and the BaGa₄Se₇ crystal length is chosen to be 10 mm. Moreover, the calculation methods employed in this study can be applied to various optical parametric oscillators and optical parametric amplifiers beyond BaGa₄Se₇-OPO/OPA.

At present, several research groups have provided Sellmeier equations for BaGa₄Se₇ crystals [21–23]. Kato et al. [24] fitted the Sellmeier equation with data obtained from second harmonic generation (SHG) and sum frequency generation (SFG) experiments using a CO₂ laser, which is considered to be more consistent with the actual conditions in the longwave range [25]. Consequently, the calculations in this paper adopt the Sellmeier equation derived by Kato et al.:

$$\begin{aligned} n_x^2 &= 6.72431 + \frac{0.26375}{\lambda^2 - 0.04248} + \frac{602.97}{\lambda^2 - 749.87} \\ n_y^2 &= 6.86603 + \frac{0.26816}{\lambda^2 - 0.04259} + \frac{682.97}{\lambda^2 - 781.78} \\ n_z^2 &= 7.16709 + \frac{0.32681}{\lambda^2 - 0.06973} + \frac{731.86}{\lambda^2 - 790.16} \end{aligned} \tag{3}$$

(0.901 ≤ λ ≤ 10.5910)

Based on the principles of energy conservation, the refractive index equation, and the Sellmeier equation, the Type-I phase matching curve for BaGa₄Se₇ crystal with a 1030 nm laser pumping is calculated and depicted in Figure 1.

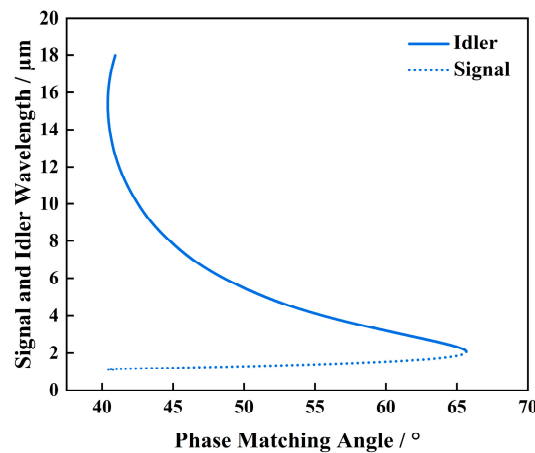


Figure 1. The Type-I phase-matching curve of BaGa₄Se₇ with 1030 nm pumping.

2.2. Phase-Mismatch

Under ideal conditions, considering the pump light, signal light, and idler light as slowly varying, with their amplitudes remaining constant after reaching a steady state, we can derive the amplitude of the idler light at the output end of the nonlinear crystal based on the three-wave mixing equation:

$$A_i(L) = \frac{2id_{\text{eff}}\omega_i A_p A_s^*}{n_i c} \left(\frac{e^{i\Delta k L} - 1}{i\Delta k} \right) \tag{4}$$

L represents the length of the crystal. The expression for optical intensity under ideal conditions can be deduced from Equation (4).

$$I_i = \frac{2d_{\text{eff}}^2 \omega_i^2 I_p I_s}{n_p n_s n_i \epsilon_0 c^3} L^2 \sin^2 \left(\frac{\Delta k L}{2} \right) \tag{5}$$

3. Calculation of the Spectrum Output Characteristics

3.1. The Influence of Pump Linewidth on the Output Spectrum

In ideal conditions, the pump source is monochromatic; however, in practice, pump sources typically have a certain linewidth. Consequently, the calculated phase-matching curves differ for different pump light frequencies, and even at the same phase-matching angle, the resulting idler wave varies, leading to the broadening of the output spectrum.

The effect of the pump source linewidth $\Delta\lambda_p$ on the variation in the idler light linewidth $\Delta\lambda_i$ can be calculated according to the following equation [19]:

$$\Delta\lambda_i = \frac{\lambda_i^2 \left(n_p - n_s + \lambda_p \frac{\partial n_p}{\partial \lambda_p} - \lambda_s \frac{\partial n_s}{\partial \lambda_s} \right)}{\lambda_p^2 \left(n_i - n_s + \lambda_i \frac{\partial n_i}{\partial \lambda_i} - \lambda_s \frac{\partial n_s}{\partial \lambda_s} \right)} \Delta\lambda_p \tag{6}$$

Equation (6) allows for estimating the impact of the pump light linewidth on the idler light’s spectral width. However, the variation in the spectral line shape is not simply a result of transverse uniform stretching. The pump light linewidth affects the idler light’s spectral characteristics by influencing the phase mismatch. The phase-matching relationship is modified and expressed as follows:

$$\Delta k = 2\pi \left(\frac{n_p^{(m)}}{\lambda_p^{(m)} + \Delta\lambda_p} - \frac{n_s^{(n)}}{\lambda_s^{(n)} + \Delta\lambda_s^{(n)}} - \frac{n_i^{(n)}}{\lambda_i^{(n)} + \Delta\lambda_i^{(n)}} \right) (m = 1, 2, \dots, n = 1, 2, \dots) \tag{7}$$

Based on Equations (6) and (7), the micro-element method is employed for infinite approximation to calculate the contribution of spectral lines contained in the pump light to the idler light’s spectrum. The pump light with a spectral width $\Delta\lambda_p$ is divided into m frequency components, and the idler light is also treated with the micro-element method, dividing $\Delta\lambda_i$ into n frequency components. By summing up the contributions of different frequency components of the pump light to a specific frequency component of the idler light, the intensity of the idler light at that frequency point can be obtained:

$$I'_i = \sum_1^m I_i \tag{8}$$

By repeating the aforementioned calculation for each frequency point of the idler light, the idler light’s spectrum can be obtained.

3.2. The Influence of Pump Divergence Angle on the Output Spectrum

In practical situations, the pump light has a certain divergence angle, and pump light from different directions corresponds to different phase-matching angles inside the nonlinear crystal, resulting in different output idler frequencies.

A straightforward estimation method is calculating the slope at the phase-matching angle corresponding to the center wavelength of the pump source from the phase-matching curve. Subsequently, the obtained slope is multiplied by the pump source’s divergence angle inside the crystal to determine the increase in the idler wave’s linewidth:

$$\Delta\lambda = \frac{d\lambda}{d\theta} \frac{\Delta\theta_{ext}}{n_p} \tag{9}$$

When accurately calculating the spectral waveform, based on the phase mismatch and the modified phase matching relationship (Equation (7)), the micro-element method is also employed. The crystal’s internal pump light is divided into multiple sub-beams based on angles, and the contribution of each sub-beam pump light to different frequencies of the idler wave is calculated. Finally, the contributions of the pump light at different angles to the idler light at a specific frequency point are summed to obtain the intensity of the idler light at that frequency point.

The calculation of the output spectrum based on OPA should consider the linewidth and divergence angle of the signal light. However, In Tian et al.’s experiment [12], the signal light is formed by focusing a small fraction of the pump into a YAG crystal to generate a stable supercontinuum through single filamentation, and this broadband signal light covers 1050–1450 nm. Therefore, in the process of optical parametric amplification, the pump light with high energy dominates the impact on the idler light instead of the signal light with low energy. Besides, the signal light is a continuous spectrum, and its linewidth is much wider than the pump light linewidth. In this situation, it is the linewidth of the pump light that determines the spectral characteristics of the output idler light, so the effect of the linewidth and divergence angle of the signal light on the output idler light is not considered in this paper.

3.3. The Influence of the Walk-Off Effect on the Output Spectrum

The walk-off angle can be determined by calculating the angle between the electric field vector E and the electric displacement field D of the light wave. For the Type-I phase matching in the BaGa₄Se₇ crystal concerned in this paper, the walk-off angle of idler light is

$$\beta^s(\lambda_i) = \arccos[e_x^s(\lambda_i)d_x^s(\lambda_i) + e_y^s(\lambda_i)d_y^s(\lambda_i) + e_z^s(\lambda_i)d_z^s(\lambda_i)] \tag{10}$$

where $e^s(\lambda_i)$ is the electric field intensity unit vector of the slow light wave, and $d^s(\lambda_i)$ is the electric displacement vector of the slow light. By utilizing the above equation, the walk-off angle of the signal and idler waves in the BaGa₄Se₇ crystal can be calculated, as shown in Figure 2.

Considering the walk-off effect, this paper provides a modified optical intensity formula for the idler light:

$$I_i = \frac{2d_{eff}^2\omega_i^2 I_p I_s}{n_p n_s n_i \epsilon_0 c^3 \cos^4 \beta_i} L^2 \sin^2 \left(\frac{\Delta k L}{2} \right) \tag{11}$$

In the equation, β_i represents the walk-off angle of the idler light within the crystal.

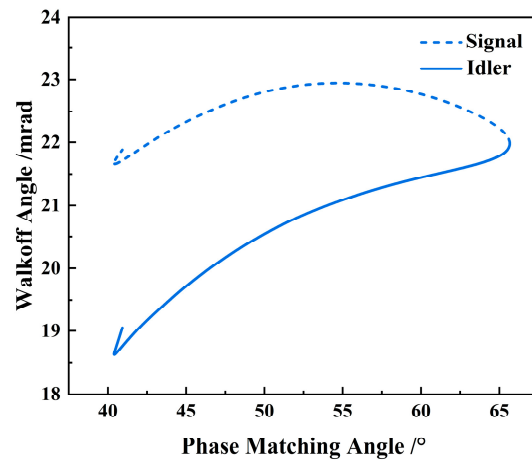


Figure 2. The walk-off angle for Type-I phase matching in BaGa₄Se₇ crystal.

3.4. The Influence of Absorption Loss of the Crystal on the Output Spectrum

The transmittance curves of different BaGa₄Se₇ crystals are all different, so when calculating the output spectral characteristics of OPO/OPA, it is essential to use the specific crystal’s absorbance curve for accurate output spectral waveform calculation. For comparison, this study utilizes the transmittance data of BaGa₄Se₇ crystals reported by Tian et al. [12], as shown in Figure 3.

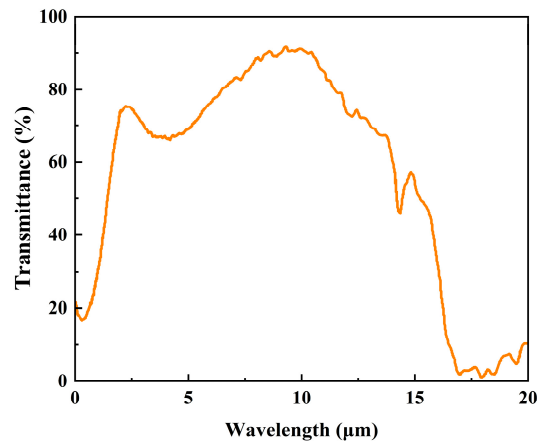


Figure 3. Transmittance curve of the BaGa₄Se₇ crystal [12] Tian, 2022.

According to the transmittance of the specific BaGa₄Se₇ crystal, the absorption coefficient of the crystal for different wavelengths can be calculated using the following absorption coefficient calculation [26]:

$$\alpha = -\frac{1}{L} \ln \left(\left\{ \left[\frac{(1-R)^2}{2TR^2} \right]^2 + \frac{1}{R^2} \right\}^{1/2} - \frac{(1-R)^2}{2TR^2} \right) \quad (12)$$

where L is the thickness of the sample, T is the transmittance, $R = (n - 1)^2 / (n + 1)^2$ is the Fresnel power reflection coefficient, and n is divided into a fast light refractive index and slow light refractive index according to the phase-matching type; the value of n can be calculated using the Sellmeier equation.

The calculated absorption coefficient curve of the BaGa₄Se₇ crystal from 2 to 18 μm is shown in Figure 4:

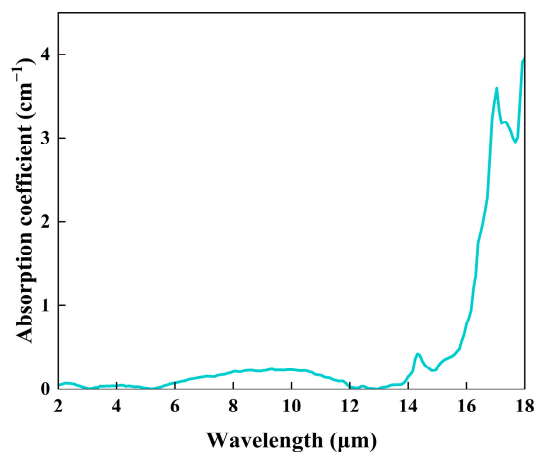


Figure 4. Absorption coefficient curve of the BaGa₄Se₇ crystal.

Considering the absorption loss of the crystal for the output spectrum, according to the Lambert–Beer–Bouguer law, the intensity of the outgoing light after passing through a certain medium is

$$I = I_0 e^{-\alpha L} \tag{13}$$

where I_0 denotes the incident light intensity, L denotes the thickness of the light beam passing perpendicularly through the medium layer, and α is the absorption coefficient of the medium for the monochromatic light.

4. Results and Discussion

Assuming that the pump light is collimated and monochromatic, and there is no walk-off effect and crystal absorption loss under ideal conditions, starting from the phase-matching characteristics of the nonlinear crystal itself, the output spectrum of the idler light centered at a specific frequency point can be obtained by calculating the phase mismatch factor for adjacent frequencies. Figure 5 shows the calculated output spectrum of the normalized idler light under ideal conditions:

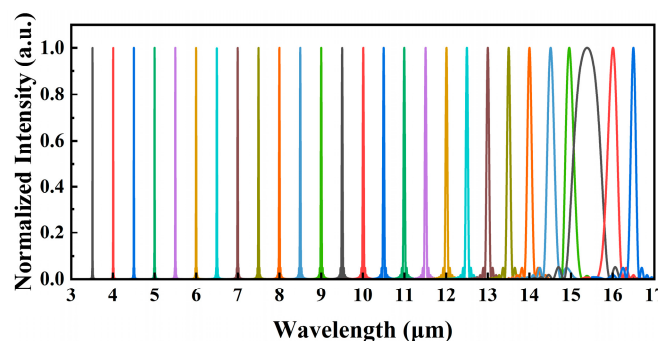


Figure 5. Output spectrum of idler light under ideal conditions.

Figure 5 illustrates the trend of the idler light’s spectral linewidth, which initially increases and then decreases with wavelength increment. This behavior can be attributed to the phase-matching curve’s slope, which gradually increases and then decreases from medium to long wavelengths. At a wavelength of 15.5 μm, the idler light exhibits its maximum spectral linewidth. This behavior is attributed to the large slope of the phase matching curve around 15.5 μm, resulting in low sensitivity of the phase mismatch factor to wavelength changes. Consequently, energy output can be obtained over a relatively wide wavelength range.

As an illustrative example at 10 μm, we analyze the impact of the pump light linewidth and pump light divergence angle on the output idler light using Equations (5)–(9). By

employing Equations (7), (8), (10), and (11), we calculate the influence of the crystal’s walk-off effect on the output idler light. The effect of the crystal’s absorption loss on the output idler light can be determined by calculating the light attenuation at different wavelengths after passing through a specific length of the crystal, utilizing Equation (13) in conjunction with the crystal absorption coefficient curve shown in Figure 4. As an illustration, we focus on 16 μm , where the absorption coefficient varies greatly, to assess the impact of the crystal’s absorption loss on the output idler light.

Figure 6 illustrates the influence of four factors on the idler output spectrum.

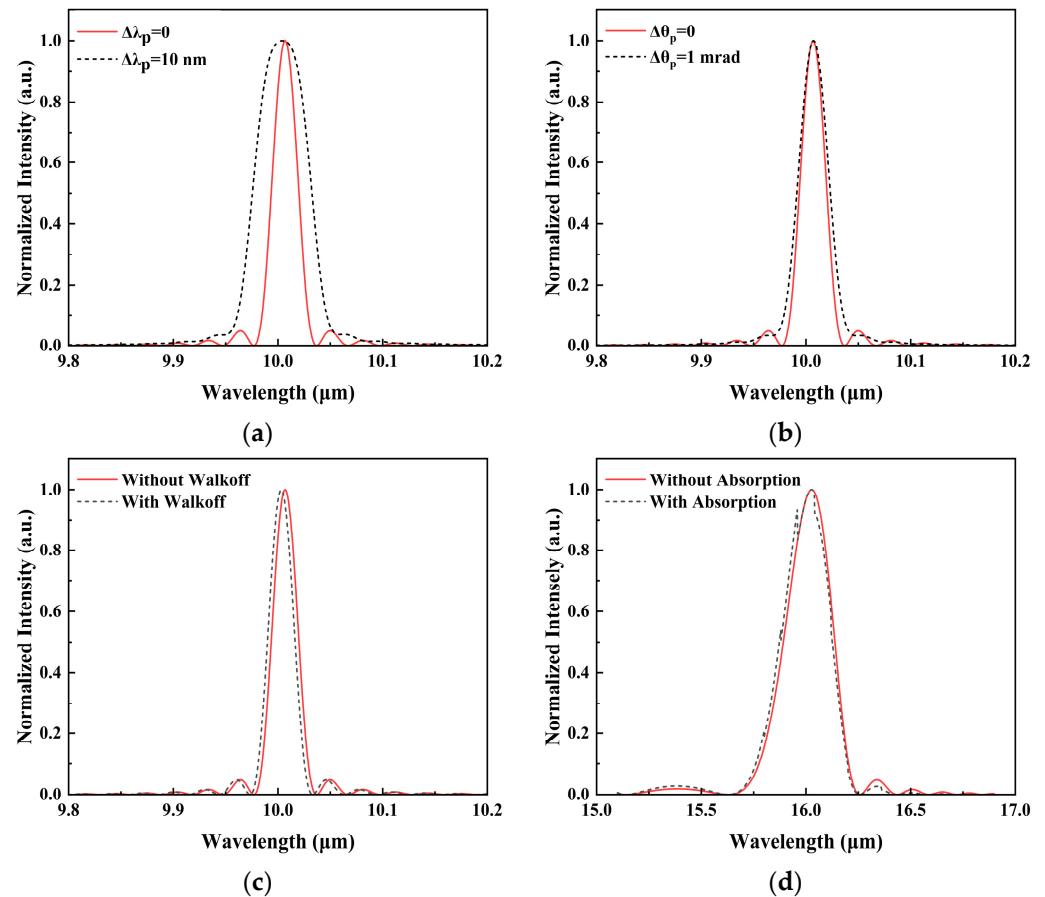


Figure 6. The effect of four factors on the output spectrum of the idler light: (a) the effect of pump linewidth on the output spectrum; (b) the effect of pump divergence angle on the output spectrum; (c) the effect of walk-off effect on the output spectrum; (d) the effect of absorption loss on the output spectrum.

In Figure 6a, when the pump linewidth is 10 nm, the idler light’s spectral characteristics are depicted by the dashed line. The spectral line exhibits broadening with non-uniform stretching characteristics, and the original sidelobes are filled in due to the contribution of the pump light at various frequency points after superimposing the microelement.

In Figure 6b, when the pump light divergence angle is 1 mrad, the effect on the output spectrum of the idler light is depicted by the dashed line. After considering the pump light divergence angle, the linewidth of the idler light slightly increases, and the shape of the spectral line undergoes changes. Additionally, the gutter of the original sidelobes is filled, which results from the superposition of the pump light’s contribution at different angles to each frequency point of the idler light. Nevertheless, it can be observed that a 1 mrad divergence angle has a relatively minor impact on the spectral line broadening. In actual experimental conditions, the pump light’s divergence angle is typically not large, as a larger divergence angle would lead to lower conversion efficiency.

In Figure 6c, the dashed line depicts the effect of the walk-off angle on the output spectrum of the 10 μm idler light without considering the pump source factor. It is observed that the linewidth of the idler light remains almost unchanged after considering the walk-off angle, but the central frequency point of the wavelength is shifted. Different frequency points correspond to different walk-off angles, all of which are milliradian magnitude, with the $\cos^4\beta$ values close to 1. Consequently, the walk-off angle has almost no impact on the light intensity, and as a result, it barely affects the linewidth of the idler light. Nevertheless, due to the presence of the walk-off angle, the phase-matching angle is slightly shifted, which causes the wavelength center to have a slight deviation.

The impact of crystal absorption on the output spectrum’s shape is evident from the dashed line in Figure 6d. As the crystal’s absorption varies at different frequency points, it alters the light intensity at those points, resulting in a non-smooth spectral line. It is essential to emphasize that, when considering absorption loss, the light intensity at specific frequency points surpasses that in the ideal state. This phenomenon arises from the normalization of spectra both before and after taking absorption loss into account. The crystal’s absorption loss induces diverse variations in the spectral shape for different center frequencies. Therefore, when calculating the output spectrum of BaGa₄Se₇-OPO/OPA, it is essential to consider the crystal’s absorption loss to accurately depict the output spectral characteristics.

The influence of different pump light linewidths and divergence angles on the idler light linewidth at different wavelengths is depicted in Figure 7.

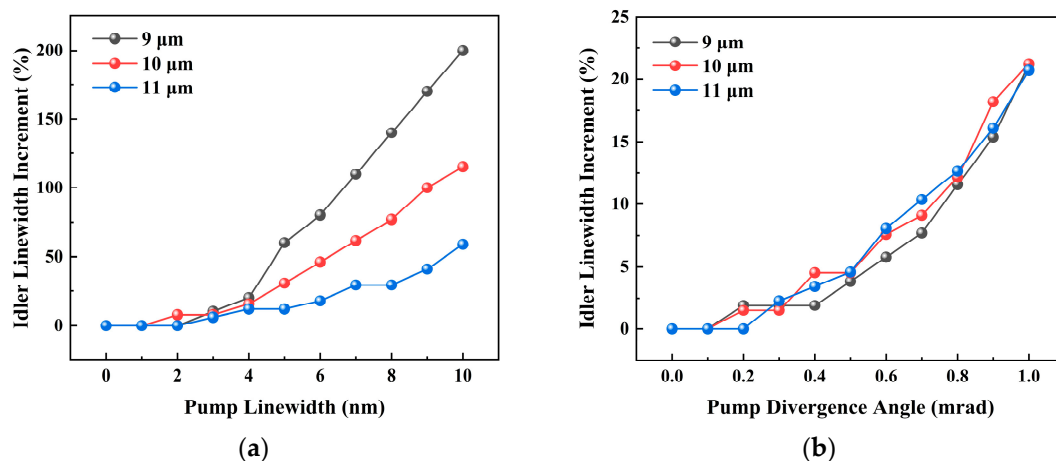


Figure 7. Effect of the different pump lights on the output spectrum: (a) different pump linewidth; (b) different pump divergence angle.

As shown in Figure 7a, when the idler light is at 9 μm, the change in pump light linewidth causes a particularly noticeable variation in the idler light linewidth increment. When the idler light is at 11 μm, the effect of pump light linewidth changes on the idler light linewidth increment is relatively minor. This phenomenon occurs because as the wavelength increases, the phase matching curve’s slope becomes greater, leading to a reduced impact of pump light linewidth changes on the idler light linewidth.

As shown in Figure 7b, the response of different idler wavelengths to different pump light divergence angles is nearly identical, and there is no significant difference in the linewidth increment. According to the phase-matching curve in Figure 1, it can be observed that in the 9–11 μm wavelength range, the slope of the phase-matching curve is almost the same. Therefore, when the divergence angle changes by the same amount, the linewidth increment in the idler light in this wavelength range remains relatively constant. However, for wavelength ranges with significantly different slopes in the phase-matching curve, the same pump light divergence angle will lead to varying impacts on the linewidth of the idler light at different wavelengths.

In order to validate the accuracy of the proposed method and compare with the measured spectral data more intuitively, the output spectrum of BaGa₄Se₇-OPA at 3.7–16.5 μm was calculated by summing up the four influencing factors based on the aforementioned method and compared with the measured spectrum and simulated spectrum of Tian et al. [12], as shown in Figure 8.

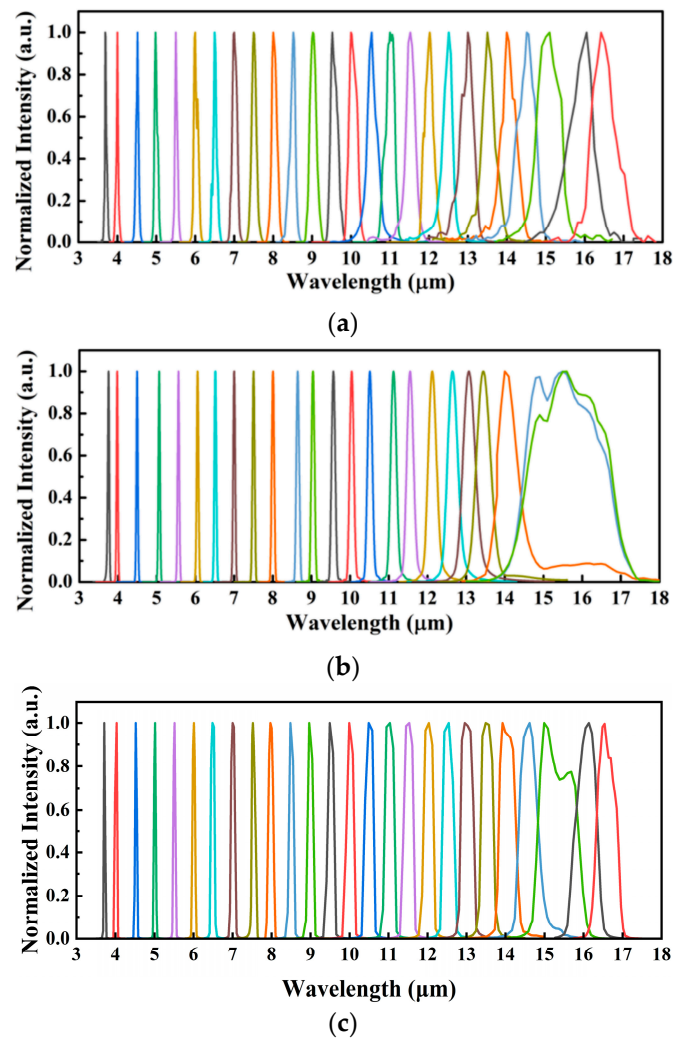


Figure 8. The 3.7–16.5 μm spectrum: (a) Spectrum measured by Tian et al. [12]; (b) Spectrum simulated by Tian et al. [12]; (c) Spectrum obtained in this study.

In Figure 8, (a) and (b) represent the experimental and simulated results from Tian et al., respectively, while (c) shows the simulated results obtained in this study. It can be observed that the measured spectral lines (a) gradually widen from short-wave to long-wave, reaching the widest at 15 μm, and then narrow slightly. The simulated spectral lines (b) also show a gradual increase but with broad continuous spectra observed at 15 μm and 16 μm, which is quite different from the measured spectrum (a). The calculated results (c) from this study demonstrate a trend of gradual increase from short wave to long wave, reaching the widest at 15 μm before narrowing down. Overall, the trend in the calculated results (c) is consistent with the measured spectrum (a). Due to the lack of detailed crystal coating parameters provided by Tian et al. in their paper, the effect of crystal coating on the output spectrum was not considered in the simulation calculations of this study. This could be a reason for the slight discrepancies between the computed results and the actual output spectrum. In Figure 8, it is evident that the calculated results (c) of this study exhibit

a closer agreement with the measured output spectrum (a), validating the effectiveness of the proposed method.

Figure 9 compares the linewidths of the measured and simulated spectra from Tian et al. with the calculated linewidths presented in this study. Upon analyzing the linewidths, it is evident that the calculated results in this paper better match the measured output spectrum. However, the simulated waveform at 15 μm appears slightly wider than the measured waveform, possibly due to the Sellmeier equation provided by Kato et al. being less accurate in the vicinity of 15 μm .

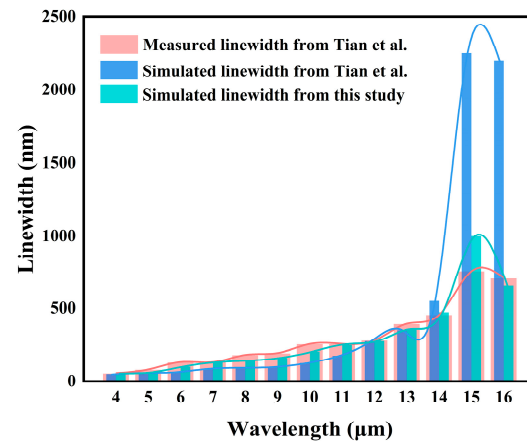


Figure 9. Comparison of the measured and simulated spectral linewidths data from Tian et al. [12] with the spectral linewidths calculated in this paper.

5. Conclusions

This paper presents a computational method regarding the output spectral characteristics of OPO/OPA systems, comprehensively considering four influencing factors: the pump light linewidth, pump light divergence angle, walk-off effect, and crystal absorption loss. Employing the micro-element method with infinite approximation, a detailed description of the output spectral distribution characteristics for OPO/OPA systems is obtained. By comparing with the experimental and simulated output spectra from Tian et al., it is evident that the results obtained using the method proposed in this paper align more closely with the experimental data, affirming the accuracy of this approach. This method allows for the simulation of output spectral characteristics that better match the actual situation and can serve as a basis for selecting gain segments in cascade amplification, enabling improved matching between OPO/OPA systems and amplifiers to generate high-energy, narrow-pulse long-wave lasers, meeting the requirements of specific applications. Furthermore, this method can be extended to calculate the output spectrum of other nonlinear crystals. In practical experiments, crystals are typically coated with anti-reflection films. Therefore, in future simulations, it is essential to consider the impact of crystal coating on the output spectrum of a coated nonlinear crystal to achieve more precise calculations.

This research contributes to a better understanding of the characteristics of OPO/OPA output spectra and provides valuable guidance for the practical application of nonlinear crystals in various laser systems.

Author Contributions: Conceptualization, Y.Z. and Y.L. (Yu Liu); methodology, Y.L. (Yu Liu); software, Y.L. (Yu Liu) and T.W.; validation, Z.Z.; formal analysis, J.B.; investigation, H.W.; resources, Z.L. and J.T.; data curation, T.W.; writing—original draft preparation, Y.L. (Yu Liu); writing—review and editing, Y.Z.; visualization, Y.L. (Yue Lu); supervision, Y.Z.; project administration, R.T.; funding acquisition, Y.Z., X.S. and C.K. All authors have read and agreed to the published version of the manuscript.

Funding: This research was funded by the Open Fund of Science and Technology on Particle Transport and Separation Laboratory, grant number QT210005; the National Natural Science Foundation

of China, grant number 61975205; and the Key Research and Development Project of the Ministry of Science and Technology of China, grant number 2020YFF0400700.

Institutional Review Board Statement: Not applicable.

Informed Consent Statement: Not applicable.

Data Availability Statement: Not applicable.

Conflicts of Interest: The authors declare no conflict of interest.

References

- Waynant, R.W.; Adams, A.R.; Elliott, C.T.; Krier, A.; Murnin, B.N.; Ilev, I.K.; Gannot, I. Mid-infrared laser applications in medicine and biology. *Philos. Trans. R. Soc.* **2001**, *359*, 635–644. [[CrossRef](#)]
- de Cumis, M.S.; Viciani, S.; Borri, S.; Patimisco, P.; Sampaolo, A.; Scamarcio, G.; De Natale, P.; D'amato, F.; Spagnolo, V. Widely-tunable mid-infrared fiber-coupled quartz-enhanced photoacoustic sensor for environmental monitoring. *Opt. Express* **2014**, *22*, 28222–28231. [[CrossRef](#)]
- Neinavaz, E.; Schlerf, M.; Darvishzadeh, R.; Gerhards, M.; Skidmore, A.K. Thermal infrared remote sensing of vegetation: Current status and perspectives. *Int. J. Appl. Earth Obs. Geoinf.* **2021**, *102*, 102415. [[CrossRef](#)]
- Bekman, H.H.P.T.; Heuvel, J.C.V.D.; Putten, F.J.M.V.; Schleijsen, R. Development of a mid-infrared laser for study of infrared countermeasures techniques. *Proc. SPIE-Int. Soc. Opt. Eng.* **2004**, *5615*, 27–38.
- Maidment, L.; Schunemann, P.G.; Reid, D.T. Molecular fingerprint-region spectroscopy from 5 to 12 μm using an orientation-patterned gallium phosphide optical parametric oscillator. *Opt. Lett.* **2016**, *41*, 4261–4264. [[CrossRef](#)] [[PubMed](#)]
- Luo, X.; Li, Z.; Guo, Y.; Yao, J.; Wu, Y. Recent Progress on New Infrared Nonlinear Optical Materials with Application Prospect. *J. Solid. State Chem.* **2019**, *270*, 674–687. [[CrossRef](#)]
- Yao, J.; Mei, D.; Bai, L.; Lin, Z.; Yin, W.; Fu, P.; Wu, Y. BaGa₄Se₇: A New Congruent-Melting IR Nonlinear Optical Material. *Inorg. Chem.* **2010**, *49*, 9212–9216. [[CrossRef](#)] [[PubMed](#)]
- Yao, J.; Yin, W.; Feng, K.; Li, X.; Mei, D.; Lu, Q.; Ni, Y.; Zhang, Z.; Hu, Z.; Wu, Y. Growth and characterization of BaGa₄Se₇ crystal. *J. Cryst. Growth* **2012**, *346*, 1–4. [[CrossRef](#)]
- Zhang, X.; Yao, J.; Yin, W.; Zhu, Y.; Wu, Y.; Chen, C. Determination of the nonlinear optical coefficients of the BaGa₄Se₇ crystal. *Opt. Express* **2015**, *23*, 552–558. [[CrossRef](#)]
- Yelissev, A.; Lobanov, S.; Krinitsin, P.; Isaenko, L. The optical properties of the nonlinear crystal BaGa₄Se₇. *Opt. Mater.* **2020**, *99*, 109564. [[CrossRef](#)]
- Yang, K.; Yao, B.; Li, C.; Yao, J.; Mi, S.; Tang, J.; Wei, D.; Li, J.; Xiao, H.; Duan, X.; et al. High efficiency non-critical phase-matching 9.3–10.6 μm optical parametric oscillator in BaGa₄Se₇ crystal. *Opt. Laser Technol.* **2023**, *160*, 109082. [[CrossRef](#)]
- Tian, K.; Wang, W.; Li, C.; Wan, Z.; Hu, B.; He, L.; Xiang, M.; Yao, J.; Wu, H.; Liang, H. Ultrabroad (3.7–17 μm) tunable femtosecond optical parametric amplifier based on BaGa₄Se₇ crystal. *Opt. Lett.* **2022**, *47*, 5973–5976. [[CrossRef](#)] [[PubMed](#)]
- Guan, M.; Chen, D.; Hu, S.; Zhao, H.; You, P.; Meng, S. Theoretical insights into ultrafast dynamics in Quantum Materials. *Ultrafast Sci.* **2022**, *2022*, 9767251. [[CrossRef](#)]
- Zhang, Z.; Zhang, J.; Chen, Y.; Xia, T.; Wang, L.; Han, B.; He, F.; Sheng, Z.; Zhang, J. Bessel terahertz pulses from superluminal laser plasma filaments. *Ultrafast Sci.* **2022**, *2022*, 9870325. [[CrossRef](#)]
- Li, X.; Huang, X.; Han, Y.; Chen, E.; Guo, P.; Zhang, W.; An, M.; Pan, Z.; Xu, Q.; Guo, X.; et al. High-performance γ -MnO₂ dual-core, pair-hole fiber for ultrafast photonics. *Ultrafast Sci.* **2023**, *3*, 0006. [[CrossRef](#)]
- Liu, X.; Yao, X.; Cui, Y. Real-time observation of the buildup of soliton molecules. *Phys. Rev. Lett.* **2018**, *121*, 023905. [[CrossRef](#)]
- Liu, X.; Pang, M. Revealing the buildup dynamics of Harmonic Mode-locking states in Ultrafast Lasers. *Laser Photonics Rev.* **2019**, *13*, 1800333. [[CrossRef](#)]
- Liu, X.; Popa, D.; Akhmediev, N. Revealing the Transition Dynamics from Q Switching to Mode Locking in a Soliton Laser. *Phys. Rev. Lett.* **2019**, *123*, 093901. [[CrossRef](#)]
- Bosenberg, W.R. Development of the Beta-Barium Metaborate Optical Parametric Oscillator. Ph.D. Thesis, Cornell University, Ithaca, NY, USA, 1990.
- Born, M.; Wolf, E. *Principles of Optics*, 1st ed.; Pergamon Press: Oxford, UK, 1959; 678p.
- Yang, F.; Yao, J.-Y.; Xu, H.-Y.; Zhang, F.-F.; Zhai, N.-X.; Lin, Z.-H.; Zong, N.; Peng, Q.-J.; Zhang, J.-Y.; Cui, D.-F.; et al. Midinfrared Optical Parametric Amplifier With 6.4–11 μm Range Based on BaGa₄Se₇. *IEEE Photonics Technol. Lett.* **2015**, *27*, 1100–1103. [[CrossRef](#)]
- Boursier, E.; Segonds, P.; Ménaert, B.; Badikov, V.; Panyutin, V.; Badikov, D.; Petrov, V.; Boulanger, B. Phase-matching directions and refined Sellmeier equations of the monoclinic acentric crystal BaGa₄Se₇. *Opt. Lett.* **2016**, *41*, 2731–2734. [[CrossRef](#)]
- Badikov, V.; Badikov, D.; Shevyrdyaeva, G.; Tyazhev, A.; Marchev, G.; Panyutin, V.; Petrov, V.; Kwasniewski, A. Phase-matching properties of BaGa₄S₇ and BaGa₄Se₇: Wide-bandgap nonlinear crystals for the mid-infrared. *Phys. Status Solidi Rapid Res. Lett.* **2010**, *5*, 31–33. [[CrossRef](#)]
- Kato, K.; Miyata, K.; Petrov, V. Phase-matching properties of BaGa₄Se₇ for SHG and SFG in the 0.901–10.5910 μm range. *Appl. Opt.* **2017**, *56*, 2978–2981. [[CrossRef](#)] [[PubMed](#)]

25. Zhao, B.; Chen, Y.; Yao, B.; Yao, J.; Guo, Y.; Wang, R.; Dai, T.; Duan, X. High-efficiency, tunable 8–9 μm BaGa₄Se₇ optical parametric oscillator pumped at 2.1 μm . *Opt. Mater. Express* **2018**, *8*, 3332–3337. [[CrossRef](#)]
26. Tochitsky, S.Y.; Petukhov, V.O.; Gorobets, V.A.; Churakov, V.V.; Jakimovich, V.N. Efficient continuous-wave frequency doubling of a tunable CO₂ laser in AgGaSe₂. *Appl. Opt.* **1997**, *36*, 1882–1888. [[CrossRef](#)] [[PubMed](#)]

Disclaimer/Publisher’s Note: The statements, opinions and data contained in all publications are solely those of the individual author(s) and contributor(s) and not of MDPI and/or the editor(s). MDPI and/or the editor(s) disclaim responsibility for any injury to people or property resulting from any ideas, methods, instructions or products referred to in the content.